Research Article

Nano Research
2021, 14(12): 4740–4747

ISSN 1998-0124 CN 11-5974/O4
https://doi.org/10.1007/s12274-021-3416-5

A highly efficient Fe-doped Ni_3S_2 electrocatalyst for overall water splitting

Min Wang[1], Li Zhang[2], Jialiang Pan[1], Meirong Huang[1], and Hongwei Zhu[1] (✉)

[1] *State Key Lab of New Ceramics and Fine Processing, School of Materials Science and Engineering, Tsinghua University, Beijing 100084, China*

[2] *Key Laboratory of Photochemical Conversion and Optoelectronic Materials, Technical Institute of Physics and Chemistry, Chinese Academy of Sciences, Beijing 100190, China*

Received: 12 December 2020 / **Revised:** 27 January 2021 / **Accepted:** 22 February 2021

ABSTRACT

The development of efficient and stable electrocatalysts with earth-abundant elements for both oxygen evolution reaction (OER) and hydrogen evolution reaction (HER) in the same electrolyte is incontrovertibly vital in water electrolysis. However, their large-scale fabrication remains a great challenge. Here, we report a self-supported electrocatalyst in the form of Fe-doped Ni_3S_2 nanoparticles *in-situ* grown on three-dimensional (3D) conductive Fe-Ni alloy foam (Fe-Ni_3S_2/AF) by surface-assisted chemical vapor transport (SACVT) method. Homogeneous growth environment and scalability of SACVT method allow Fe-Ni_3S_2 nanoparticles uniformly growing on AF in large-scale. Fe-Ni_3S_2/AF exhibits high activity and durability when act as HER catalyst and OER precatalyst in alkaline media. The HER and OER overpotential at 10 mA/cm^2 is considerably small, only 75 and 267 mV, respectively. Moreover, the electrolyzer assembled by Fe-Ni_3S_2/AF for overall water splitting exhibits a low cell voltage and high durability in long-term test. Based on experiments and theoretical calculation, the significantly enhanced activity could be originated from the incorporation of Fe, which contributed to increase the electrochemical active surface area, enhance electrical conductivity, optimize the hydrogen and H_2O adsorption energy of Ni_3S_2 (101) surface in HER, and form active bimetallic Ni-Fe(oxy)hydroxide in OER. The excellent durability of self-supported Fe-Ni_3S_2/AF could be benefited from the *in-situ* growth of Fe-Ni_3S_2 nanoparticles on 3D AF, which could ensure closely mechanical adhesion between active materials and substrate, promote charge transport and increase surface area. This work provides a facile method for large-scale synthesis of electrocatalysts with high activity and long-term durability for efficient water electrolysis in alkaline media.

KEYWORDS

sulfide, surface-assisted chemical vapor transport, large-scale, *in-situ* growth, overall water splitting

1 Introduction

Hydrogen energy, as a renewable, sustainable and clean energy, its development and application are of great significance for solving energy shortage and environmental degradation issues [1]. Electrochemical water splitting is a sustainable and efficient strategy for hydrogen generation benefiting from abundant and inexhaustible water resources, high-purity H_2 production and zero carbon emission [2]. Currently, Pt-based materials and Ir/Ru oxides remain the state-of-the-art electrocatalysts for hydrogen evolution reaction (HER) and oxygen evolution reaction (OER), respectively, but scarcity and high cost of these noble metals considerably impede the large-scale application of water electrolysis technology [3, 4]. Thus, it is imperative to explore earth-abundant alternatives to precious metals as efficient electrocatalysts to satisfy the rapid development of the hydrogen economy [5, 6]. Tremendous efforts have been devoted to develop highly active alternatives such as metal oxides [7, 8], sulfides [9–11], selenides [12, 13], and phosphides [14, 15] in electrochemical OER or HER. To get minimized overpotentials, water splitting should be performed in either strong alkaline or acidic electrolyte. However, a challenge for most of these earth-abundant electrocatalysts is that a highly active electrocatalyst in acidic electrolyte may be inert or even unstable in basic electrolyte, like MoS_2 [16], and metal oxides for OER are usually not stable in acidic electrolyte [17]. Therefore, efficient and stable electrocatalysts with earth-abundant elements for both HER and OER conveniently in the same electrolyte to sustained overall water splitting still need to be further explored.

Nickel sulfides (e.g., NiS, NiS_2 and Ni_3S_2), especially Ni_3S_2, has received increasing attention in electrochemical overall water splitting because of its abundant resources, facile preparation and potential electrocatalytic performance in both electrocatalytic HER and OER [18, 19]. Unfortunately, the application of Ni_3S_2 in water electrolysis has been distinctly restricted by its mediocre electrocatalytic activity caused by its low intrinsic conductivity and instability in alkaline electrolytes caused by corrosion. As we know, the kinetics of HER in alkaline electrolytes and OER with multi-step proton-coupled electron transfer processes are both sluggish [20, 21]. To further improve the electrocatalytic performance of Ni_3S_2, metal-doping has been proved to be an effective strategy by numerous theoretical efforts and experimental studies [22, 23]. Especially, the element

Address correspondence to hongweizhu@tsinghua.edu.cn

Fe is a good dopant in Ni_3S_2, which could greatly enhance electrocatalytic performance by modulating the coordination valence states, enhancing electronic conductivity, and optimizing hydrogen/water adsorption energy [24, 25]. Additionally, *in-situ* growth of active electrocatalysts on a conductive substrate as self-supported electrodes could effectively boost the electrocatalytic activity and durability by greatly promoted charge transport and enhanced mechanical adhesion [2, 9].

However, large-scale preparation of Fe-doped Ni_3S_2 structures with good quality *in-situ* grown on a highly conductive substrate as self-supported electrodes still remains attractive and challenging. On one hand, the relatively complex synthetic way is a bottleneck for developing metal-doped Ni_3S_2 integrated electrodes because of the majority of these electrocatalysts are prepared by two-step hydrothermal or solvothermal methods, usually tedious and time-consuming [26]. On another hand, the obtained metal-doped Ni_3S_2 structures generally exhibit poor purity and crystallinity due to the use of aqueous or organic solvents [27, 28]. Therefore, a facile method allowing uniform *in-situ* growth of Fe-doped Ni_3S_2 materials and large-scale preparation on conductive substrates is urgently needed.

Herein, we report *in-situ* growth of Fe-doped Ni_3S_2 nanoparticles on a three-dimensional (3D) conductive Fe-Ni alloy foam (denoted as Fe-Ni_3S_2/AF) by one-step surface-assisted chemical vapor transport (SACVT) method. Typically, Fe-Ni AF and a certain amount of sulfur powders are sealed together in a quartz ampoule with high-vacuum and followed by a facile heating step. The large-scale and uniform growth of Fe-Ni_3S_2 nanoparticles on the surface of 10 cm × 10 cm alloy foam is benefited from the homogeneous growth environment and scalability of SACVT method. Fe-Ni AF could provide the reaction source of Fe and Ni element and act as the conductive substrate to form self-supported Fe-Ni_3S_2/AF electrode simultaneously, whose 3D porous structure could also provide a larger electrochemical surface area and promote sufficiently exposure of the active sites available for electrochemical redox reactions on Fe-Ni_3S_2 nanoparticles. *In-situ* growth of active Fe-Ni_3S_2 nanoparticles on Fe-Ni AF could observably enhance the mechanical adhesion and promote charge transport of electrocatalyst, leading to improved electrocatalytic durability and activity. Simultaneously, the incorporation of Fe in Ni_3S_2 could greatly increase the electrochemical active surface area, electrical conductivity, optimize the hydrogen and H_2O adsorption energy of Ni_3S_2 (101) surface in HER, and form active bimetallic Ni-Fe(oxy)hydroxide in OER, leading to a dramatically enhanced activity for overall water splitting. Notably, the as-prepared Fe-Ni_3S_2/AF electrodes exhibit both highly efficient activity for HER and OER in 1.0 M KOH. The HER and OER overpotential at 10 mA/cm^2 is considerably small, only 75 and 267 mV, respectively. Furthermore, the overall water splitting electrolyzer assembled by Fe-Ni_3S_2/AF as HER catalyst and OER precatalyst owns low cell voltage and high durability in long-term test (100 h). This work provides a facile and useful preparation method to expand the application of nickel-based electrocatalysts with excellent activity and long-term durability in overall water splitting with large-scale.

2 Results and discussion

2.1 Preparation and characterizations

The schematics for preparation of Fe-Ni_3S_2 nanoparticles by SACVT method is shown in Fig. 1(a). The detail was described in the experimental section. Simply, Fe-Ni AF and a spot of sulfur powders were sealed in a quartz ampoule in vacuum and then heated at 400 °C for 10 min. Fe-Ni AF was

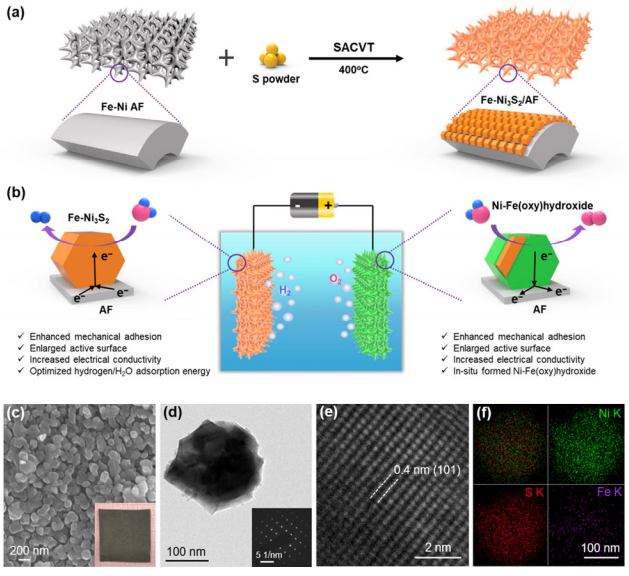

Figure 1 (a) Schematics for preparation of Fe-Ni_3S_2 nanoparticles on AF by SACVT method. (b) Two-electrode configuration of Fe-Ni_3S_2/AF for overall water splitting. (c) SEM image of Fe-Ni_3S_2 nanoparticles. Inset shows the photograph of Fe-Ni_3S_2/AF. (d) TEM image and SAED pattern, (e) HRTEM image, and (f) chemical mappings of Ni, S and Fe species of a Fe-Ni_3S_2 nanoparticle.

applied as the reactive source of Fe and Ni and the 3D conductive substrate for nucleation and growth of Fe-Ni_3S_2 nanoparticles simultaneously. Increasing the size of the quartz ampoule and Fe-Ni AF can obtain self-supported electrodes with large-scale. In SACVT method, one-step sulfidation of Fe-Ni AF could ensure that *in-situ* growth of Fe-doped Ni_3S_2 nanoparticles, and a small amount of sulfur powder added could allow a thin self-supported film of Fe-Ni_3S_2 nanoparticles grown on the surface of alloy foam uniformly. Incorporation of Fe and *in-situ* growth on substrate could dramatically improve the activity and durability of self-supported Fe-Ni_3S_2/AF electrode. 3D porous structure of Fe-Ni AF could provide larger electrochemical surface area and more exposed active sites on active Fe-Ni_3S_2 nanoparticles [29].

The morphology and structure of Fe-Ni_3S_2 nanoparticles are shown in Figs. 1(c)–1(f) zoomed in step by step. The surface of Fe-Ni AF after reaction is grayish brown and very uniform on the whole as shown in the inset of Fig. 1(c), and the surface of Fe-Ni AF is fully covered with Fe-Ni_3S_2 nanoparticles with size of about 200 nm. The photograph of the initial Fe-Ni AF and Fe-Ni AF after reaction in the quartz ampoule are shown in Fig. S1 in the Electronic Supplementary Material (ESM). Transmisson electron microscopy (TEM) image further demonstrates the formation of Fe-Ni_3S_2 nanoparticles with the morphology of nanoparticle and the inset selected area electron diffraction (SAED) pattern indicates the good crystallinity of Fe-Ni_3S_2 nanoparticles as shown in Fig. 1(d). The high-resolution TEM (HRTEM) image taken from the Fe-Ni_3S_2 nanoparticle is shown in Fig. 1(e), exhibiting clear lattice fringes with an interplanar distance of 0.4 nm which can be indexed to the (101) plane of Ni_3S_2 phase. Furthermore, as shown in Fig. 1(f) and Fig. S2(a) in the ESM, elemental mapping technique and X-ray energy dispersive spectrum (EDS) were applied to verify the element distribution of Fe-Ni_3S_2 nanoparticles. It's clearly seen that Ni, S and Fe elements distributed on the surface of Fe-Ni AF and the atomic ratio of Ni to S is estimated to be about 3:2. Moreover, as shown in Fig. S2(b) in the ESM, the atomic percent of Fe element in Fe-Ni_3S_2 nanoparticles from EDS data is about 3%, which is slightly lower than the atomic percent of Fe element in Fe-Ni AF.

The crystallinity and phase of as-prepared Fe-Ni_3S_2 nanoparticles on Fe-Ni AF were further investigated by the X-ray diffraction (XRD) as shown in Fig. S3 in the ESM. The diffraction peaks can be well indexed as Ni_3S_2 (PDF No. 44-1418). Figure S4(a) in the ESM presents that other two large peaks at 44.4° and 51.7° are originated from Fe-Ni AF, and no peaks attributed to Fe sulfides can be detected, indicating Fe could be existed in the lattice of Ni_3S_2 with a doping state. The scanning electron microscopy (SEM) images and XRD patterns of Ni_3S_2/NF and FeS_x/IF are shown in the Fig. S4 in the ESM, which also strongly support the view that Fe acts as a dopant in Ni_3S_2. Additionally, the surface elemental compositions and valence states of Fe-Ni_3S_2 nanoparticles were characterized by X-ray photoelectron spectroscopy (XPS) as presented in Fig. S5 in the ESM and Fig. 5(c). The high-resolution Ni 2p region spectrum exhibits the peak at 873.6 eV with a satellite at 879.3 eV attributed to Ni^{2+} $2p_{1/2}$ and the peak at 855.8 eV with a satellite at 861.0 eV attributed to Ni^{2+} $2p_{3/2}$. Moreover, the signals at 870.0 and 852.8 eV can be assigned to metallic Ni peaks [30]. In Fe 2p region spectrum, the obvious peaks at 724.5 and 712.2 eV can be ascribed to Fe $2p_{1/2}$ and Fe $2p_{3/2}$ with no satellite peaks were detected, suggesting iron element exists in the form of Fe^{3+} [27]. The S^{2-} $2p_{1/2}$ and S^{2-} $2p_{3/2}$ are observed at 163.5 and 162.3 eV in S 2p spectrum attributing to metal-sulfur bonding [23]. Interestingly, a slightly negative shift happened in the peaks of S 2p of Fe-Ni_3S_2/AF when compared with pure Ni_3S_2/NF (163.7 and 162.5 eV) as shown in Fig. S6 in the ESM, implying an extra electron transfer to S in Fe-Ni_3S_2 [24]. The electronegativity of Fe is 1.83, which is lower than that of Ni (1.91), thus the electron transfer from Fe to neighboring S is much easier than that from Ni and S [24], which could also support the existence of doped Fe in Fe-Ni_3S_2/AF.

All of the above results definitely proved that we successfully prepared Fe-Ni_3S_2 nanoparticles on the Fe-Ni AF by one-step SACVT method.

2.2 Electrocatalytic performance of HER

The electrocatalytic HER performance of Fe-Ni_3S_2 nanoparticles on Fe-Ni AF (Fe-Ni_3S_2/AF) was measured using a typical three-electrode cell in N_2-saturated 1.0 M KOH aqueous solution with a scan rate of 5 mV/s. For comparison, Ni_3S_2 on Ni foam (Ni_3S_2/NF) and FeS_x on Fe foam (FeS_x/IF) samples were also investigated under the same conditions. The linear sweep voltammetry (LSV) curves of these samples and Pt/C-NF electrodes are shown in Fig. 2(a). It's obviously seen that Fe-Ni_3S_2/AF electrode owns the best HER property with a low overpotential of 75 mV to reach 10 mA/cm^2 current density, which is much smaller than that of 177 and 277 mV of FeS_x/IF and Ni_3S_2/NF electrodes, respectively. The comparison with non-doped Ni_3S_2 and FeS_x strongly confirms the beneficial effect of Fe doping in Ni_3S_2 for overall water splitting. Meantime, as shown in Fig. S7(a) in the ESM, the electrocatalytic activity of Fe-Ni_3S_2/AF for HER is significantly better than Fe-Ni AF that applied as the conductive substrate. Furthermore, the lowest Tafel slope in Fig. 2(b) suggests that Fe-Ni_3S_2/AF electrode owns faster HER kinetics progress than FeS_x/IF and Ni_3S_2/NF electrodes. The electrochemically active surface areas (ECSA) of these electrodes were measured from the electrochemical double-layer capacitance of the electrocatalytic surface by cyclic voltammograms in a non-Faradaic region [31]. The specific capacitances of Fe-Ni_3S_2/AF, FeS_x/IF and Ni_3S_2/NF electrodes calculated from the slope of the linear fitting were 15.2, 5.2, and 3.8 mF/cm^2, respectively, as shown in Fig. 2(c) and Fig. S8 in the ESM. Based on the reported typical specific capacitances, the specific capacitance for a flat surface was assumed as 40 μF/cm^2 for 1 cm^2 of the real surface area in 1 M KOH, then the ECSA could be calculated by the equation ECSA = specific capacitance (mF/cm^2)/(40 μF/cm^2 per cm^2) [31, 32]. The estimated ECSAs for Fe-Ni_3S_2/AF, FeS_x/IF and Ni_3S_2/NF were 380, 130, and 95 cm^2, respectively. As can be seen, the ECSA of Fe-Ni_3S_2/AF is much higher than that of Ni_3S_2/NF and FeS_x/IF electrodes, implying more active sites available for electrochemical redox reactions on the surface of Fe-Ni_3S_2 nanoparticles. All these results manifest that the significantly boosted electrocatalytic activity toward HER of Fe-Ni_3S_2/AF is mainly ascribed to the doping of Fe element. Compared to other comparable works, no matter element-doped nickel sulfides (e.g., V-NiS_2 [33], N-Ni_3S_2 [18], Fe-NiS_2 [34]), iron-nickel sulfide [25, 35], or even Co/Ni-based mixed metal-organic nanosheet array [36], our Fe-Ni_3S_2/NF electrode possesses better electrocatalytic activity for HER as shown in Fig. 2(d). The detail information of these electrodes was listed in Table S1 in the ESM.

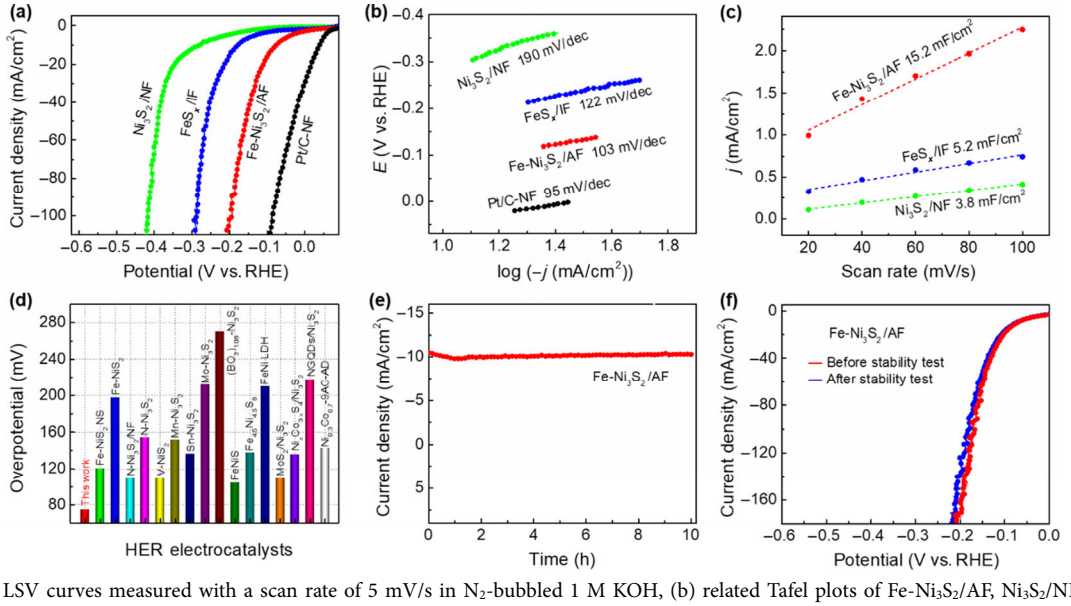

Figure 2 (a) LSV curves measured with a scan rate of 5 mV/s in N_2-bubbled 1 M KOH, (b) related Tafel plots of Fe-Ni_3S_2/AF, Ni_3S_2/NF, FeS_x/IF and Pt/C-NF. (c) Linear fittings of the capacitive current densities at different scan rates of Fe-Ni_3S_2/AF, Ni_3S_2/NF and FeS_x/IF. (d) HER overpotentials (10 mA/cm^2) of Fe-Ni_3S_2/AF electrode and reported HER electrocatalysts for comparison. (e) Long-term electrochemical HER test, and (f) LSV curves before and after long-term HER test of Fe-Ni_3S_2/AF electrode.

Furthermore, durability is another important criterion to judge an advanced electrocatalyst for HER. The current density of Fe-Ni_3S_2/AF electrode was monitored at a constant voltage for 10 h under continuous HER operation as shown in Fig. 2(e). The curve of current density versus time keeps stable by and large. As for the initial drop, it may mainly attribute to the shielding effect of H_2 bubbles generated on the Fe- Ni_3S_2/AF electrode continuously and the limited mass-transfer between electrolyte and electrode. The high durability of Fe-Ni_3S_2/AF electrode can also be confirmed by the comparison of LSV curves before and after electrochemical durability test, there is no significant degradation happened in Fig. 2(f). The enhanced mechanical adhesion between active Fe-Ni_3S_2 and 3D Fe-Ni AF substrate results in the excellent electrocatalytic durability, which is originated from the *in-situ* growth of Fe-Ni_3S_2 nanoparticles on the 3D conductive substrate.

To understand the intrinsic reasons for the improved HER activity arising from the Fe-doping, the electronic structures and adsorption characters of Fe-Ni_3S_2 and Ni_3S_2 were calculated by density functional theory (DFT) method as shown in Fig. 3. The model was built based on (101) surface and three possible Fe-doping sites were considered with substituted energy of +0.48, +0.44, and +0.47 eV for site 1, 2, and 3, respectively (as shown in Fig. S9 in the ESM). Thus, further calculations were all based on the most stable configuration of 2 due to its lowest substituted energy, as shown in Fig. 3(a). Firstly, the density of states (DOS) of Fe-Ni_3S_2 and Ni_3S_2 were calculated, as shown in Fig. 3(b). The continuous states crossing Fermi level reveal that the metallic behavior of Ni_3S_2 can be maintained after Fe-doping, indicating a high conductivity of Fe-Ni_3S_2. On the whole, the DOS of Fe-Ni_3S_2 has a slight tendency to migrate to higher energy levels, which could strengthen the adsorption of small molecules on the surface. Generally, the adsorption free energy of H* (ΔG_{H^*}) on the electrocatalyst can be employed as a good descriptor for its HER activity [37]. The calculated ΔG_{H^*} on Ni and S sites of Fe-Ni_3S_2 and Ni_3S_2 (101) surfaces were demonstrated in Fig. 3(c). Obviously, the ΔG_{H^*} on Ni sites are much lower than that on S sites, indicating that Ni atoms on the (101) surface are the main active sites for HER in both Fe-Ni_3S_2 and Ni_3S_2. Moreover, the ΔG_{H^*} on Ni site can be decreased from 0.63 to 0.61 eV after Fe-doping, representing the optimized adsorption of hydrogen on Fe-Ni_3S_2 (101) surface. More importantly, the adsorption of H_2O on the active surface

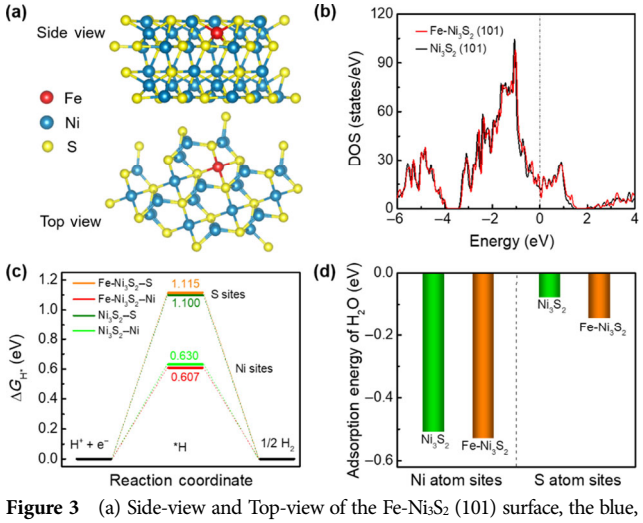

Figure 3 (a) Side-view and Top-view of the Fe-Ni_3S_2 (101) surface, the blue, yellow and red spheres represent Ni, S and Fe atoms, respectively. (b) Calculated density of states of the (101) surfaces of Ni_3S_2 and Fe-Ni_3S_2. (c) Calculated free-energy diagram of HER over the (101) surfaces of Ni_3S_2 and Fe-Ni_3S_2. (d) Calculated water adsorption energy of Ni_3S_2 and Fe-Ni_3S_2.

plays a vital role in alkaline media, because a sluggish water activation process may be the rate-determining step in HER. The water adsorption energy could be applied as an evaluation for the energy barrier of water activation on the electrocatalysts [38]. As shown in Fig. 3(d), the water adsorption energy on Ni and S sites of Fe-Ni_3S_2 are –0.53 and –0.14 eV, which are lower than that of Ni_3S_2 (–0.51 and –0.08 eV), respectively, demonstrating that water activation process could happen on the surface of Fe-Ni_3S_2 more easily to start the HER. The metallic behavior and optimized adsorption energy for hydrogen and H_2O of Fe-Ni_3S_2 are both beneficial for improving the HER activity of self-supported Fe-Ni_3S_2/AF electrode.

The excellent electrocatalytic HER performance of Fe-Ni_3S_2/AF electrode is attributed to the successful preparation of Fe-Ni_3S_2 nanoparticles on 3D alloy foam with *in-situ* doping of Fe element by SACVT method, as shown in Fig. 1(b). Firstly, Fe-Ni_3S_2/AF electrode owns higher electrical conductivity and faster charge transfer benefited from the self-supported structure obtained from *in-situ* growth. Secondly, Fe element doping and 3D porous structure of Fe-Ni AF substrate could increase the ECSA, which is indicative of more active sites and improved electrocatalytic activity. More importantly, Fe element doping would greatly optimize the ability for adsorption of H* and H_2O molecule in the electrocatalytic reaction [24], which would further increase the intrinsic activity of active sites [25, 34]. Finally, the enhanced mechanical adhesion between active Fe-Ni_3S_2 nanoparticles and conductive Fe-Ni AF substrate would ensure the stability of Fe-Ni_3S_2/AF electrode during long-term test, which is mainly originated from the *in-situ* growth of active materials on the substrate.

2.3 Electrocatalytic performance of OER

The electrocatalytic OER performance of Fe-Ni_3S_2/AF electrode was examined by a typical three-electrode cell in 1.0 M KOH purged with N_2. As shown in Fig. 4(a), the electrocatalytic OER activities of Fe-Ni_3S_2/AF, Ni_3S_2/NF, FeS_x/IF and IrO_2-NF electrodes were measured through LSV curves with a scan rate of 5 mV/s. The overpotential of Fe-Ni_3S_2/AF electrode at a current density of 10 mA/cm^2 is 267 mV, which considerably lower than Ni_3S_2/NF electrode (350 mV), FeS_x/IF electrode (380 mV), and even IrO_2-NF electrode. Metal sulfides would transform into metal (oxy)hydroxide during OER, so Fe-Ni_3S_2/AF electrode would give rise to more active bimetallic Ni-Fe (oxy)hydroxide during OER test under oxidizing potentials, while Ni_3S_2/NF electrode and FeS_x/IF electrode could only generate single component Ni (oxy)hydroxide and Fe (oxy)hydroxide [39, 40]. It's also the reason for we named Fe-Ni_3S_2/AF as OER precatalyst due to Ni-Fe (oxy)hydroxide actually responsible for the electrocatalytic OER [41]. Meanwhile, the electrocatalytic activity of Fe-Ni_3S_2/AF for OER is also obviously higher than the conductive substrate Fe-Ni AF, as shown in Fig. S7(b) in the ESM. Significantly, the tafel slope of Fe-Ni_3S_2 nanoparticles is approximately 36 mV/dec, which is greatly lower than that of Ni_3S_2/NF (55 mV/dec) and FeS_x/IF (100 mV/dec) electrodes in Fig. 4(b). In other words, the incorporation of Fe element in Ni_3S_2 could improve the electrocatalytic OER activity and activate water-oxidation reaction kinetics. Meantime, a much smaller charge transfer resistance of Fe-Ni_3S_2/AF electrode in Fig. 4(c) illustrates a faster electron transfer, benefitting from the change of electronic properties after Fe doping in Ni_3S_2.

By contrast, the Fe-Ni_3S_2/AF electrode owns lower overpotential (at 10 mA/cm^2) and smaller Tafel slope comparing with related electrode materials reported previously in Fig. 4(d), like metal-doped Ni_3S_2 [27, 33, 26], iron-nickel sulfide [42], Ni_3S_2 composites [43], and CoFe layered double hydroxide [44].

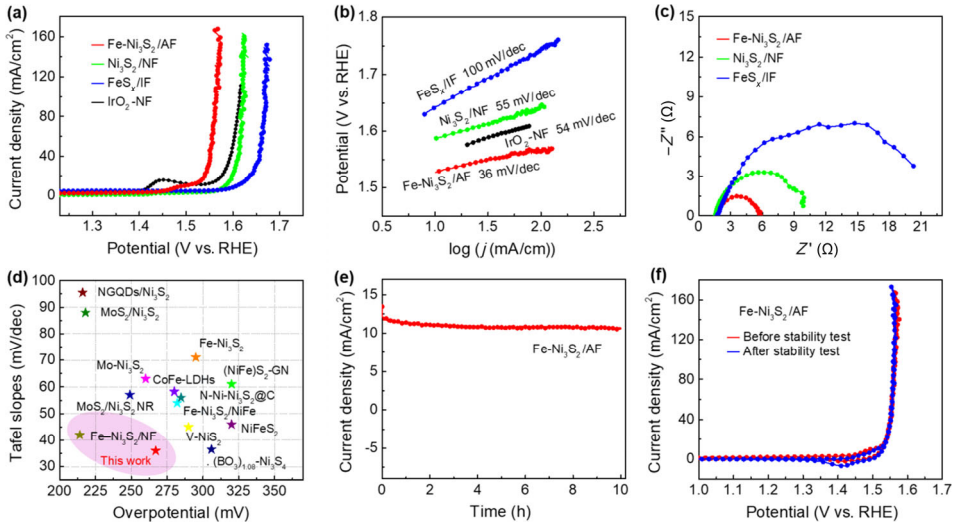

Figure 4 (a) LSV curves measured with a scan rate of 5 mV/s in N_2-bubbled 1 M KOH, (b) corresponding Tafel slopes of Fe-Ni_3S_2/AF, Ni_3S_2/NF, FeS_x/IF and IrO_2-NF. (c) Electrochemical impedance spectra of Fe-Ni_3S_2/AF, Ni_3S_2/NF and FeS_x/IF. (d) OER overpotentials (at 10 mA/cm^2) and Tafel slopes of Fe-Ni_3S_2/AF electrode and reported OER electrocatalysts for comparison. (e) Long-term electrochemical OER test, and (f) CV curves before and after long-term OER test of Fe-Ni_3S_2/AF electrode.

More detailed information of these electrodes was listed in Table S2 in the ESM. To assess the electrochemical OER durability of Fe-Ni_3S_2/AF electrode, a long-term water oxidation test was conducted in 1 M KOH media under constant potential test. Figures 4(e) and 4(f) show that it still remained steady OER electrocatalytic activity even after 10 h test. We attribute the superior electrocatalytic durability of Fe-Ni_3S_2/AF electrode to the *in-situ* growth of Fe-Ni_3S_2 nanoparticles on Fe-Ni AF as self-supported electrode without any binder or conductive additive.

Fe-Ni_3S_2/AF as OER precatalyst exhibits superior electrocatalytic activity and durability as shown in Fig. 1(b). On one hand, Fe doping could generate bimetallic Ni-Fe (oxy)hydroxide during OER test under high potential, which is more active than single component Ni(oxy)hydroxide. On another hand, introduction of Fe element could increase electrical conductivity of Fe-Ni_3S_2/AF electrode and 3D porous structure of electrode could promote the exposure of active sites and accelerate the electrolyte penetration. Finally, *in-situ* growth of Fe-Ni_3S_2 nanoparticles on Fe-Ni AF could greatly improve the electrocatalytic stability of whole self-supported electrode due to the large mechanical adhesion force.

2.4 Overall water splitting

To evaluate the electrocatalytic activity toward overall water splitting, a two-electrode configuration was assembled by Fe-Ni_3S_2/AF electrodes as both cathode and anode electrodes, the inset in Fig. 5(a). Impressively, Fe-Ni_3S_2/AF electrodes exhibit

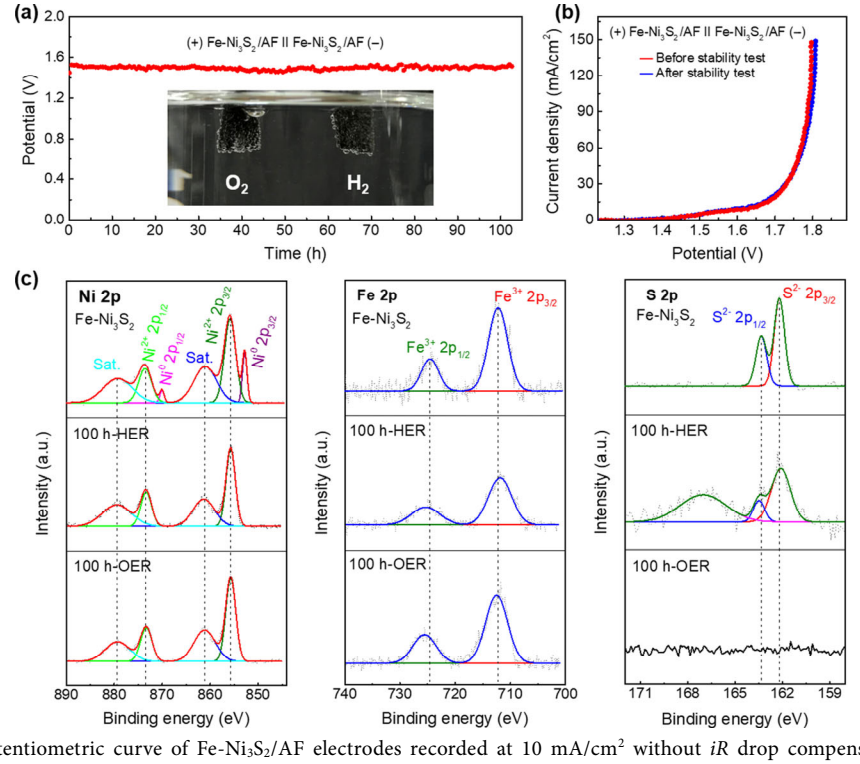

Figure 5 (a) Chronopotentiometric curve of Fe-Ni_3S_2/AF electrodes recorded at 10 mA/cm^2 without *iR* drop compensation. (b) LSV curves of Fe-Ni_3S_2/AF electrodes before and after chronopotentiometry test. (c) High-resolution XPS spectra of Ni 2p, Fe 2p and S 2p for initial state, after 100-h HER test, and after 100-h OER test of Fe-Ni_3S_2/AF electrodes.

a superior durability with negligible degradation in a period of 100 h by the chronoamperometry at the current density of 10 mA/cm^2 in Fig. 5(a). The nearly overlapped LSV curves before and after long-term durability test in Fig. 5(b) also confirms its stable activity for overall water splitting in alkaline media. The superior durability of Fe-Ni_3S_2/AF electrode results mainly from the strong adhesion between *in-situ* grown Fe-Ni_3S_2 nanoparticles and Fe-Ni AF. Compared with conventional powdery electrocatalysts, the self-supported Fe-Ni_3S_2/AF electrode doesn't need additional binder, exhibiting seamless contact and tight integration that could prevent the shedding of active electrocatalysts caused by the ceaseless generation of gas bubbles during the reaction. As shown in Figs. S10(a) and S10(b) in the ESM, the surface morphology of Fe-Ni_3S_2/AF was well maintained after hydrogen evolution for 100 h, while some new subtle structures appeared on the surface of Fe-Ni_3S_2 nanoparticles after 100 h OER test. Notably, the content of oxygen element of Fe-Ni_3S_2/AF after OER durability test increases considerably, as shown in Fig. S10(d) in the ESM. According to the reaction mechanism of oxygen evolution in water splitting, we inferred that Ni-Fe (oxy)hydroxide *in-situ* formed on the surface of Fe-Ni_3S_2/AF during oxygen evolution, which would be responsible for the electrocatalysis of OER actually.

To further confirm this point, the samples of Fe-Ni_3S_2/AF after HER and OER durability test were probed by surface-sensitive XPS technique, as shown in Fig. 5(c). For Ni 2p, after HER and OER durability test for 100 h, the XPS peaks related to Ni^{2+} exhibit no obvious change, while the peaks related to metallic Ni^0 are significantly attenuated. For XPS spectrum of Fe 2p, the peaks of Fe-Ni_3S_2/AF after OER durability test exhibit a positive shift compared with the as-prepared Fe-Ni_3S_2/AF, while the peaks of Fe-Ni_3S_2/AF after HER durability test show no obvious positive shift. The positive shift strongly suggests near-surface of Fe-Ni_3S_2 would convert to Ni-Fe (oxy)hydroxide during the oxygen evolution process. Meanwhile, the change of S 2p XPS spectrum could also support this transformation confirmedly. The peaks assigned to S^{2-} $2p_{1/2}$ and S^{2-} $2p_{3/2}$ can still be probed after HER durability test, together with the peak centered at about 167 eV corresponding to sulfate formed during HER test [24]. However, no peaks of S 2p could be detected after OER durability test due to the change of elements composition in near surface region of Fe-Ni_3S_2 nanoparticles. In addition, the XRD peaks of Fe-Ni_3S_2/AF are both well maintained after long-term HER and OER durability test, as shown in Fig. S11 in the ESM. The reason for no diffraction peaks detected in XRD pattern could be explained by the low content and crystallinity of Ni-Fe (oxy)hydroxide formed on the near surface of Fe-Ni_3S_2/AF.

In brief, the near-surface of Fe-Ni_3S_2 nanoparticles would be converted to Ni-Fe (oxy)hydroxide during oxygen evolution process actually, but well-maintained during hydrogen evolution process. Namely, Fe-Ni_3S_2 acted as HER catalyst and OER precatalyst in hydrogen and oxygen evolution, respectively, and they both behaved excellent electrocatalytic durability.

3 Conclusions

In summary, we prepared Fe-Ni_3S_2 nanoparticles *in-situ* grown on 3D conductive Fe-Ni AF with large-scale by one-step SACVT method, which could be directly utilized as self-supported electrocatalysts for overall water splitting. Homogeneous growth environment and scalability of SACVT method allowed Fe-Ni_3S_2 nanoparticles growing uniformly on the surface of Fe-Ni AF on a large scale. When applied as HER catalyst, Fe-Ni_3S_2/AF exhibited low overpotential of 75 mV at a current density of 10 mA/cm^2, small Tafel slope of 103 mV/dec in alkaline media. When catalyzed OER process, Fe-Ni_3S_2/AF acted as precatalyst because of the near-surfaces of Fe-Ni_3S_2 nanoparticles were converted to Ni-Fe (oxy)hydroxide that actually responsible for the OER catalysis. Low overpotential of 267 mV at 10 mA/cm^2 and extremely small Tafel slope of 36 mV/dec confirmed its high electrocatalytic activity for OER. Moreover, Fe-Ni_3S_2/AF presented excellent electrocatalytic activity and long-term durability when assembled into the overall water splitting electrolyzer. The incorporation of Fe element in Ni_3S_2 significantly increased the electrochemical active surface area, enhanced electrical conductivity, optimized the hydrogen and H_2O adsorption energy in HER, and *in-situ* formed active bimetallic Ni-Fe(oxy)hydroxide in OER, leading to improved electrocatalytic activity for overall water splitting. *In-situ* growth of active Fe-Ni_3S_2 nanoparticles on conductive Fe-Ni AF ensured closely mechanical adhesion and promoted charge transport between active materials and substrate, which greatly enhanced durability of self-supported Fe-Ni_3S_2/AF electrode. The successful preparation of self-supported Fe-Ni_3S_2/AF by SACVT method gave us huge support to realize large-scale synthesis of electrocatalysts for efficient water electrolysis.

4 Experimental

4.1 Large-scale synthesis of Fe-Ni_3S_2 nanoparticles

Fe-Ni_3S_2 nanoparticles were synthesized with large-scale by one-step SACVT method mentioned in our previous work [45]. Firstly, Fe-Ni AF (14.66 g, ~10 cm × 10 cm ×1 mm) and sulfur powders (0.81 g, 99.9995%) were vacuum-sealed together in a quartz ampoule (ϕ 4 cm ×18 cm). This method exhibits good scalability as the sizes of reactor and reactive substrate could be easily regulated. Before using, Fe-Ni AF was pretreated successively with 3 M HCl, absolute ethanol and deionized water to ensure a clean surface. Secondly, the quartz ampoule was pushed quickly into the center temperature zone of a tube furnace heated to 400 °C in advance and held for 10 min. Finally, the ampoule was pushed out from the tube furnace and cooled naturally to ambient temperature. For comparison, Ni_3S_2 and FeS_x samples were prepared under same reaction condition by reacting Ni foam and Fe foam with sulfur powders, respectively.

4.2 Materials characterizations

As-prepared Fe-Ni_3S_2 nanoparticles were characterized by scanning electron microscope (SEM, MERLIN VP Compact, Carl Zeiss), transmission electron microscope (TEM, JEM-2010F), X-ray diffraction (XRD, D8 Advance, Bruker) with Cu Kα radiation, and X-ray photoelectron spectroscope (XPS, PHI Quantera II, Ulvac-Phi Inc) using Al Kα radiation ($h\nu$ = 1486.6 eV).

4.3 Electrochemical measurements

All electrochemical measurements were performed on a CHI 660E electrochemical station (CH Instruments, Inc. Shanghai). In a three-electrode system, Fe-Ni_3S_2 nanoparticles together with Fe-Ni AF were applied as the working electrode directly, taking a saturated calomel electrode (SCE) as reference electrode and a platinum sheet as counter electrode. As for carbon-supported Pt (Pt/C, 20%) and IrO_2 electrodes, the catalysts (8 mg) were dispersed in 1 mL of a 4:1 (v/v) ethanol/deionized water mixture and 20 μL Nafion solution by sonicating for more than 1 h to get a catalyst ink, and then dropped onto a piece of Ni foam and dried naturally to form Pt/C-NF and IrO_2-NF. All electrochemical tests were carried out in 1 M KOH electrolyte (pH=14) and stirred magnetically. The presented potentials

were calibrated to reversible hydrogen electrode (RHE) by the Nernst equation

$$E\,(\mathrm{RHE}) = E\,(\mathrm{SCE}) + 0.0591\mathrm{pH} + 0.241\ \mathrm{V} \quad (1)$$

LSV and CV curves with a scan rate of 5 mV/s were measured to obtain the electrocatalytic activity of electrocatalysts (results were *iR*-corrected manually, unless otherwise noted). Electrochemical impedance spectra (EIS) were recorded in the frequencies between 100 kHz and 0.01 Hz. The ECSA measurements were calculated based on the CV curves with scan rates from 20 to 100 mV/s in a non-Faradaic potential region [46]. The stability of the working electrode was evaluated by long-term HER or OER operation at a static overpotential. To explore the overall water splitting performance, chronopotentiometric stability and LSV curves were recorded in a two-electrode cell in which Fe-Ni_3S_2/AF electrodes served as both anode and cathode.

4.4 Theoretical calculation

To investigate the effect of Fe-doping on the electronic structure and adsorption energy for water and hydrogen of Ni_3S_2, the present first principle DFT calculations were performed by Vienna *Ab initio* Simulation Package (VASP) with the projector augmented wave (PAW) method [47, 48]. The exchange-functional was treated by the generalized gradient approximation (GGA) of Perdew-Burke-Ernzerhof (PBE) functional [49]. The energy cutoff for the plane wave basis expansion was set as 450 eV and the convergence threshold was set as 0.03 eV/Å in force and 10^{-4} eV in energy. The surface of Ni_3S_2 has been cut along the (101) direction, while a 15 Å vacuum layer was considered along the *z* axis for all systems to avoid the interaction between periodic structures. The Brillouin zone integration was sampled with a 3×3×1 k-point for geometric optimization. The DFT-D3 method was applied to consider the van der Waals interaction [50]. The substituted energy E_{sub} of the systems was defined as Eq. (2):

$$E_{sub} = E_{tot} + E_{Ni} - E_{pristine} - E_{Fe} \quad (2)$$

where the E_{tot} and $E_{pristine}$ are the energy of Fe-doped and pristine Ni_3S_2 system, E_{Ni} and E_{Fe} denote the energy of single metal atom in bulk materials, respectively. Free energy change (ΔG) of the reaction was calculated as follows:

$$\Delta G = \Delta E_{DFT} + \Delta E_{ZPE} - T\Delta S \quad (3)$$

where ΔE_{DFT} means the DFT electronic energy difference of each step, ΔE_{ZPE} and ΔS are the zero-point energy change and the entropy variation obtained by vibration analysis, respectively, T is the temperature (T = 300 K). The value of (ΔE_{ZPE}–$T\Delta S$) equals 0.28 eV by following the scheme proposed [51].

Acknowledgements

This work was supported by the National Key Research and Development Program of China (No. 2017YFB1104300).

Electronic Supplementary Material: Supplementary material (EDS, XPS, XRD and SEM results of the samples; electrochemical measurements of the self-supported electrodes; the possible doping sites of Fe atoms in Ni_3S_2) is available in the online version of this article at https://doi.org/10.1007/s12274-021-3416-5.

References

[1] Zou, X. X.; Zhang, Y. Noble metal-free hydrogen evolution catalysts for water splitting. *Chem. Soc. Rev.* **2015**, *44*, 5148–5180.

[2] Sun, H. M.; Yan, Z. H.; Liu, F. M.; Xu, W. C.; Cheng, F. Y.; Chen, J. Self-supported transition-metal-based electrocatalysts for hydrogen and oxygen evolution. *Adv. Mater.* **2020**, *32*, 1806326.

[3] Wang, H. T.; Lee, H. W.; Deng, Y.; Lu, Z. Y.; Hsu, P. C.; Liu, Y. Y.; Lin, D. C.; Cui, Y. Bifunctional non-noble metal oxide nanoparticle electrocatalysts through lithium-induced conversion for overall water splitting. *Nat. Commun.* **2015**, *6*, 7261.

[4] Liu, Y. Y.; Wu, J. J.; Hackenberg, K. P.; Zhang, J.; Wang, Y. M.; Yang, Y. C.; Keyshar, K.; Gu, J.; Ogitsu, T.; Vajtai, R. et al. Self-optimizing, highly surface-active layered metal dichalcogenide catalysts for hydrogen evolution. *Nat. Energy* **2017**, *2*, 17127.

[5] Arif, M.; Yasin, G.; Shakeel, M.; Mushtaq, M. A.; Ye, W.; Fang, X. Y.; Ji, S. F.; Yan, D. P. Highly active sites of NiVB nanoparticles dispersed onto graphene nanosheets towards efficient and pH-universal overall water splitting. *J. Energy Chem.* **2021**, *58*, 237–246.

[6] Arif, M.; Yasin, G.; Shakeel, M.; Fang, X. Y.; Gao, R.; Ji, S. F.; Yan, D. P. Coupling of bifunctional CoMn-layered double hydroxide@graphitic C_3N_4 nanohybrids towards efficient photoelectrochemical overall water splitting. *Chem.-Asian J.* **2018**, *13*, 1045–1052.

[7] Hutchings, G. S.; Zhang, Y.; Li, J.; Yonemoto, B. T.; Zhou, X. G.; Zhu, K. K.; Jiao, F. *In situ* formation of cobalt oxide nanocubanes as efficient oxygen evolution catalysts. *J. Am. Chem. Soc.* **2015**, *137*, 4223–4229.

[8] Ge, R. X.; Ma, M.; Ren, X.; Qu, F. L.; Liu, Z. A.; Du, G.; Asiri, A. M.; Chen, L.; Zheng, B. Z.; Sun, X. P. A $NiCo_2O_4$@Ni-Co-Ci core-shell nanowire array as an efficient electrocatalyst for water oxidation at near-neutral pH. *Chem. Commun.* **2017**, *53*, 7812–7815.

[9] Wang, M.; Zhang, L.; Huang, M. R.; Zhang, Q. F.; Zhao, X. L.; He, Y. J.; Lin, S. Y.; Pan, J. L.; Zhu, H. W. One-step synthesis of a hierarchical self-supported WS_2 film for efficient electrocatalytic hydrogen evolution. *J. Mater. Chem. A* **2019**, *7*, 22405–22411.

[10] Ren, X.; Wang, W. Y.; Ge, R. X.; Hao, S.; Qu, F. L.; Du, G.; Asiri, A. M.; Wei, Q.; Chen, L.; Sun, X. P. An amorphous $FeMoS_4$ nanorod array toward efficient hydrogen evolution electrocatalysis under neutral conditions. *Chem. Commun.* **2017**, *53*, 9000–9003.

[11] Yang, L.; Xie, L. S.; Ren, X.; Wang, Z. Q.; Liu, Z. A.; Du, G.; Asiri, A. M.; Yao, Y. D.; Sun, X. P. Hierarchical $CuCo_2S_4$ nanoarrays for high-efficient and durable water oxidation electrocatalysis. *Chem. Commun.* **2018**, *54*, 78–81.

[12] Wang, M.; Zhang, L.; Huang, M. R.; Liu, Y.; Zhong, Y. J.; Pan, J. L.; Wang, Y. R.; Zhu, H. W. Morphology-controlled tantalum diselenide structures as self-optimizing hydrogen evolution catalysts. *Energy Environ. Mater.* **2020**, *3*, 12–18.

[13] Gao, R.; Zhang, H.; Yan, D. P. Iron diselenide nanoplatelets: Stable and efficient water-electrolysis catalysts. *Nano Energy* **2017**, *31*, 90–95.

[14] Xu, J. Y.; Li, J. J.; Xiong, D. H.; Zhang, B. S.; Liu, Y. F.; Wu, K. H.; Amorim, I.; Li, W.; Liu, L. F. Trends in activity for the oxygen evolution reaction on transition metal (M = Fe, Co, Ni) phosphide pre-catalysts. *Chem. Sci.* **2018**, *9*, 3470–3476.

[15] Xu, S. R.; Zhao, H. T.; Li, T. S.; Liang, J.; Lu, S. Y.; Chen, G.; Gao, S. Y.; Asiri, A. M.; Wu, Q.; Sun, X. P. Iron-based phosphides as electrocatalysts for the hydrogen evolution reaction: Recent advances and future prospects. *J. Mater. Chem. A* **2020**, *8*, 19729–19745.

[16] Tan, Y. W.; Liu, P.; Chen, L. Y.; Cong, W. T.; Ito, Y.; Han, J. H.; Guo, X. W.; Tang, Z.; Fujita, T.; Hirata, A. et al. Monolayer MoS_2 films supported by 3D nanoporous metals for high-efficiency electrocatalytic hydrogen production. *Adv. Mater.* **2014**, *26*, 8023–8028.

[17] Smith, R. D. L.; Prévot, M. S.; Fagan, R. D.; Zhang, Z. P.; Sedach, P. A.; Siu, M. K. J.; Trudel, S.; Berlinguette, C. P. Photochemical route for accessing amorphous metal oxide materials for water oxidation catalysis. *Science* **2013**, *340*, 60–63.

[18] Chen, P. Z.; Zhou, T. P.; Zhang, M. X.; Tong, Y.; Zhong, C. G.; Zhang, N.; Zhang, L. D.; Wu, C. Z.; Xie, Y. 3D nitrogen-anion-decorated nickel sulfides for highly efficient overall water splitting. *Adv. Mater.* **2017**, *29*, 1701584.

[19] Yang, C.; Gao, M. Y.; Zhang, Q. B.; Zeng, J. R.; Li, X. T.; Abbott, A. P. *In-situ* activation of self-supported 3D hierarchically porous Ni_3S_2 films grown on nanoporous copper as excellent pH-universal electrocatalysts for hydrogen evolution reaction. *Nano Energy* **2017**, *36*, 85–94.

[20] Zhang, J.; Wang, T.; Pohl, D.; Rellinghaus, B.; Dong, R. H.; Liu, S. H.; Zhuang, X. D.; Feng, X. L. Interface engineering of MoS_2/Ni_3S_2 heterostructures for highly enhanced electrochemical overall-water-splitting activity. *Angew. Chem., Int. Ed.* **2016**, *55*, 6702–6707.

[21] Gao, R.; Yan, D. P. Recent development of Ni/Fe-based micro/nanostructures toward photo/electrochemical water oxidation. *Adv. Energy Mater.* **2020**, *10*, 1900954.

[22] Du, H. T.; Kong, R. M.; Qu, F. L.; Lu, L. M. Enhanced electrocatalysis for alkaline hydrogen evolution by Mn doping in a Ni_3S_2 nanosheet array. *Chem. Commun.* **2018**, *54*, 10100–10103.

[23] Liu, Q.; Xie, L. S.; Liu, Z. A.; Du, G.; Asiri, A. M.; Sun, X. P. A Zn-doped Ni_3S_2 nanosheet array as a high-performance electrochemical water oxidation catalyst in alkaline solution. *Chem. Commun.* **2017**, *53*, 12446–12449.

[24] Zhang, G.; Feng, Y. S.; Lu, W. T.; He, D.; Wang, C. Y.; Li, Y. K.; Wang, X. Y.; Cao, F. F. Enhanced catalysis of electrochemical overall water splitting in alkaline media by Fe doping in Ni_3S_2 nanosheet arrays. *ACS Catal.* **2018**, *8*, 5431–5441.

[25] Long, X.; Li, G. X.; Wang, Z. L.; Zhu, H. Y.; Zhang, T.; Xiao, S.; Guo, W. Y.; Yang, S. H. Metallic iron-nickel sulfide ultrathin nanosheets as a highly active electrocatalyst for hydrogen evolution reaction in acidic media. *J. Am. Chem. Soc.* **2015**, *137*, 11900–11903.

[26] Wu, C. R.; Liu, B. T.; Wang, J.; Su, Y. Y.; Yan, H. Q.; Ng, C.; Li, C.; Wei, J. M. 3D structured Mo-doped Ni_3S_2 nanosheets as efficient dual-electrocatalyst for overall water splitting. *Appl. Surf. Sci.* **2018**, *441*, 1024–1033.

[27] Yuan, C. Z.; Sun, Z. T.; Jiang, Y. F.; Yang, Z. K.; Jiang, N.; Zhao, Z. W.; Qazi, U. Y.; Zhang, W. H.; Xu, A. W. One-step *in situ* growth of iron-nickel sulfide nanosheets on FeNi alloy foils: High-performance and self-supported electrodes for water oxidation. *Small* **2017**, *13*, 1604161.

[28] Lin, Y. F.; Chen, G.; Wan, H.; Chen, F. S.; Liu, X. H.; Ma, R. Z. 2D free-standing nitrogen-doped Ni-Ni_3S_2@carbon nanoplates derived from metal-organic frameworks for enhanced oxygen evolution reaction. *Small* **2019**, *15*, 1900348.

[29] Arif, M.; Yasin, G.; Luo, L.; Ye, W.; Mushtaq, M. A.; Fang, X. Y.; Xiang, X.; Ji, S. F.; Yan, D. P. Hierarchical hollow nanotubes of NiFeV-layered double hydroxides@CoVP heterostructures towards efficient, pH-universal electrocatalytical nitrogen reduction reaction to ammonia. *Appl. Catal. B-Environ.* **2020**, *265*, 118559.

[30] Song, H.; Oh, S.; Yoon, H.; Kim, K. H.; Ryu, S.; Oh, J. Bifunctional NiFe inverse opal electrocatalysts with heterojunction Si solar cells for 9.54%-efficient unassisted solar water splitting. *Nano Energy* **2017**, *42*, 1–7.

[31] McCrory, C. C. L.; Jung, S.; Peters, J. C.; Jaramillo, T. F. Benchmarking heterogeneous electrocatalysts for the oxygen evolution reaction. *J. Am. Chem. Soc.* **2013**, *135*, 16977–16987.

[32] Li, X.; Zhang, L.; Huang, M. R.; Wang, S. Y.; Li, X. M.; Zhu, H. W. Cobalt and nickel selenide nanowalls anchored on graphene as bifunctional electrocatalysts for overall water splitting. *J. Mater. Chem. A* **2016**, *4*, 14789–14795.

[33] Liu, H. J.; He, Q.; Jiang, H. L.; Lin, Y. X.; Zhang, Y. K.; Habib, M.; Chen, S. M.; Song, L. Electronic structure reconfiguration toward pyrite NiS_2 via engineered heteroatom defect boosting overall water splitting. *ACS Nano* **2017**, *11*, 11574–11583.

[34] Yan, J. Q.; Wu, H.; Li, P.; Chen, H.; Jiang, R. B.; Liu, S. Z. Fe(III) doped NiS_2 nanosheet: A highly efficient and low-cost hydrogen evolution catalyst. *J. Mater. Chem. A* **2017**, *5*, 10173–10181.

[35] Piontek, S.; Andronescu, C.; Zaichenko, A.; Konkena, B.; Junge Puring, K.; Marler, B.; Antoni, H.; Sinev, I.; Muhler, M.; Mollenhauer, D. et al. Influence of the Fe:Ni ratio and reaction temperature on the efficiency of $(Fe_xNi_{1-x})_9S_8$ electrocatalysts applied in the hydrogen evolution reaction. *ACS Catal.* **2018**, *8*, 987–996.

[36] Ye, W.; Yang, Y. S.; Fang, X. Y.; Arif, M.; Chen, X. B.; Yan, D. P. 2D cocrystallized metal-organic nanosheet array as an efficient and stable bifunctional electrocatalyst for overall water splitting. *ACS Sustain. Chem. Eng.* **2019**, *7*, 18085–18092.

[37] Feng, L. L.; Yu, G. T.; Wu, Y. Y.; Li, G. D.; Li, H.; Sun, Y. H.; Asefa, T.; Chen, W.; Zou, X. X. High-index faceted Ni_3S_2 nanosheet arrays as highly active and ultrastable electrocatalysts for water splitting. *J. Am. Chem. Soc.* **2015**, *137*, 14023–14026.

[38] Dong, J.; Zhang, F. Q.; Yang, Y.; Zhang, Y. B.; He, H. L.; Huang, X. F.; Fan, X. J.; Zhang, X. M. (003)-Facet-exposed Ni_3S_2 nanoporous thin films on nickel foil for efficient water splitting. *Appl. Catal. B-Environ.* **2019**, *243*, 693–702.

[39] Dionigi, F.; Strasser, P. NiFe-based (oxy)hydroxide catalysts for oxygen evolution reaction in non-acidic electrolytes. *Adv. Energy Mater.* **2016**, *6*, 1600621.

[40] Trotochaud, L.; Young, S. L.; Ranney, J. K.; Boettcher, S. W. Nickel-iron oxyhydroxide oxygen-evolution electrocatalysts: The role of intentional and incidental iron incorporation. *J. Am. Chem. Soc.* **2014**, *136*, 6744–6753.

[41] Jin, S. Are metal chalcogenides, nitrides, and phosphides oxygen evolution catalysts or bifunctional catalysts? *ACS Energy Lett.* **2017**, *2*, 1937–1938.

[42] Jiang, J.; Lu, S.; Gao, H.; Zhang, X.; Yu, H. Q. Ternary $FeNiS_2$ ultrathin nanosheets as an electrocatalyst for both oxygen evolution and reduction reactions. *Nano Energy* **2016**, *27*, 526–534.

[43] Yang, Y. Q.; Zhang, K.; Lin, H. L.; Li, X.; Chan, H. C.; Yang, L. C.; Gao, Q. S. MoS_2-Ni_3S_2 heteronanorods as efficient and stable bifunctional electrocatalysts for overall water splitting. *ACS Catal.* **2017**, *7*, 2357–2366.

[44] Gao, R.; Yan, D. P. Fast formation of single-unit-cell-thick and defect-rich layered double hydroxide nanosheets with highly enhanced oxygen evolution reaction for water splitting. *Nano Res.* **2018**, *11*, 1883–1894.

[45] Wang, M.; Zhang, L.; Zhong, Y. J.; Huang, M. R.; Zhen, Z.; Zhu, H. W. *In situ* electrodeposition of polypyrrole onto $TaSe_2$ nanobelts quasi-arrays for high-capacitance supercapacitor. *Nanoscale* **2018**, *10*, 17341–17346.

[46] Wang, S. Y.; Zhang, L.; Li, X.; Li, C. L.; Zhang, R. J.; Zhang, Y. J.; Zhu, H. W. Sponge-like nickel phosphide-carbon nanotube hybrid electrodes for efficient hydrogen evolution over a wide pH range. *Nano Res.* **2017**, *10*, 415–425.

[47] Blöchl, P. E. Projector augmented-wave method. *Phys. Rev. B* **1994**, *50*, 17953–17979.

[48] Kresse, G.; Furthmüller, J. Efficiency of *ab-initio* total energy calculations for metals and semiconductors using a plane-wave basis set. *Comput. Mater. Sci.* **1996**, *6*, 15–50.

[49] Perdew, J. P.; Chevary, J. A.; Vosko, S. H.; Jackson, K. A.; Pederson, M. R.; Singh, D. J.; Fiolhais, C. Atoms, molecules, solids, and surfaces: Applications of the generalized gradient approximation for exchange and correlation. *Phys. Rev. B* **1992**, *46*, 6671–6687.

[50] Grimme, S.; Antony, J.; Ehrlich, S.; Krieg, H. A consistent and accurate *ab initio* parametrization of density functional dispersion correction (DFT-D) for the 94 elements H-Pu. *J. Chem. Phys.* **2010**, *132*, 154104.

[51] Voiry, D.; Yamaguchi, H.; Li, J. W.; Silva, R.; Alves, D. C. B.; Fujita, T.; Chen, M. W.; Asefa, T.; Shenoy, V. B.; Eda, G. et al. Enhanced catalytic activity in strained chemically exfoliated WS_2 nanosheets for hydrogen evolution. *Nat. Mater.* **2013**, *12*, 850–855.